

Article

Fabrication and Characterization of Highly Efficient As-Synthesized WO₃/Graphitic-C₃N₄ Nanocomposite for Photocatalytic Degradation of Organic Compounds

Mai S. A. Hussien^{1,2}, Abdelfatteh Bouzidi³, Hisham S. M. Abd-Rabboh^{4,5}, Ibrahim S. Yahia^{6,7,8}, Heba Y. Zahran^{6,7,8}, Mohamed Sh. Abdel-wahab^{9,*}, Walaa Alharbi¹⁰, Nasser S. Awwad⁴ and Medhat A. Ibrahim^{11,12}

- ¹ Department of Chemistry, Faculty of Education, Ain Shams University, Roxy, Cairo 11757, Egypt; maisalehamar@gmail.com
 - ² Nanoscience Laboratory for Environmental and Bio-Medical Applications (NLEBA), Department of Physics, Faculty of Education, Ain Shams University, Roxy, Cairo 11757, Egypt
 - ³ Laboratory of Materials for Energy and Environment, and Modeling (LMEEM), Faculty of Sciences of Sfax, University of Sfax, B.P. 1171, Sfax 3038, Tunisia; bouzidi.abdelfatteh@yahoo.fr
 - ⁴ Department of Chemistry, Faculty of Science, King Khalid University, P.O. Box 9004, Abha 61421, Saudi Arabia; habdrabboh@kku.edu.sa (H.S.M.A.-R.); nsawwad20@yahoo.com (N.S.A.)
 - ⁵ Department of Chemistry, Faculty of Science, Ain Shams University, Abbassia, Cairo 11566, Egypt
 - ⁶ Laboratory of Nano-Smart Materials for Science and Technology (LNSMST), Department of Physics, Faculty of Science, King Khalid University, P.O. Box 9004, Abha 61413, Saudi Arabia; dr_isyahia@yahoo.com (I.S.Y.); dr_hyzahran@yahoo.com (H.Y.Z.)
 - ⁷ Research Center for Advanced Materials Science (RCAMS), King Khalid University, P.O. Box 9004, Abha 61413, Saudi Arabia
 - ⁸ Semiconductr Laboratory, Department of Physics, Faculty of Education, Ain Shams University, Roxy, Cairo 11757, Egypt
 - ⁹ Materials Science and Nanotechnology Department, Faculty of Postgraduate Studies for Advanced Sciences, Beni-Suef University, Beni-Suef 62511, Egypt
 - ¹⁰ Department of Chemistry, Science and Arts College, Rabigh Campus, King Abdulaziz University, P.O. Box 80200, Jeddah 21589, Saudi Arabia; wnhalharbe@kau.edu.sa
 - ¹¹ Nanotechnology Research Centre (NTRC), The British University in Egypt (BUE), Suez Desert Road, El-Sherouk City 11837, Cairo, Egypt; medahmed6@yahoo.com
 - ¹² Molecular Spectroscopy and Modeling Unit, Spectroscopy Department, National Research Centre, 33 El-Bohouth St., Dokki, Giza 12622, Egypt
- * Correspondence: mshaabanct@gmail.com; Tel.: +20-155-4246-910



Citation: Hussien, M.S.A.; Bouzidi, A.; Abd-Rabboh, H.S.M.; Yahia, I.S.; Zahran, H.Y.; Abdel-wahab, M.S.; Alharbi, W.; Awwad, N.S.; Ibrahim, M.A. Fabrication and Characterization of Highly Efficient As-Synthesized WO₃/Graphitic-C₃N₄ Nanocomposite for Photocatalytic Degradation of Organic Compounds. *Materials* **2022**, *15*, 2482. <https://doi.org/10.3390/ma15072482>

Academic Editor: Andrea Petrella

Received: 21 February 2022

Accepted: 23 March 2022

Published: 28 March 2022

Publisher's Note: MDPI stays neutral with regard to jurisdictional claims in published maps and institutional affiliations.



Copyright: © 2022 by the authors. Licensee MDPI, Basel, Switzerland. This article is an open access article distributed under the terms and conditions of the Creative Commons Attribution (CC BY) license (<https://creativecommons.org/licenses/by/4.0/>).

Abstract: The incorporation of tungsten trioxide (WO₃) by various concentrations of graphitic carbon nitride (g-C₃N₄) was successfully studied. X-ray diffraction (XRD), Scanning Electron Microscope (SEM), and Diffused Reflectance UV-Vis techniques were applied to investigate morphological and microstructure analysis, diffused reflectance optical properties, and photocatalysis measurements of WO₃/g-C₃N₄ photocatalyst composite organic compounds. The photocatalytic activity of incorporating WO₃ into g-C₃N₄ composite organic compounds was evaluated by the photodegradation of both Methylene Blue (MB) dye and phenol under visible-light irradiation. Due to the high purity of the studied heterojunction composite series, no observed diffraction peaks appeared when incorporating WO₃ into g-C₃N₄ composite organic compounds. The particle size of the prepared composite organic compound photocatalysts revealed no evident influence through the increase in WO₃ atoms from the SEM characteristic. The direct and indirect bandgap were recorded for different mole ratios of WO₃/g-C₃N₄, and indicated no apparent impact on bandgap energy with increasing WO₃ content in the composite photocatalyst. The composite photocatalysts' properties better understand their photocatalytic activity degradations. The pseudo-first-order reaction constants (K) can be calculated by examining the kinetic photocatalytic activity.

Keywords: microstructure analysis; diffused reflectance UV-Vis; photocatalysis; tungsten trioxide; Methylene Blue and phenol degradations

1. Introduction

The photocatalytic performance of semiconductor materials, based on oxide semiconductors in their crystalline phases, has recently become desirable for producing hydrogen and oxygen via visible-light water splitting. Designing semiconductor composites produced between two semiconductor materials necessitates crystalline phase engineering [1–3]. The use of heterogeneous photocatalysis to convert water into hydrogen gas is regarded as one of the most promising options for addressing global energy and pollution problems [1,4,5]. In the present century, the rapid decline in energy sources, and increased power, waste, and renewable H₂ energy sources, are attributable to worldwide demand for fossil fuels. A. Fujishima et al. studied for a long time how to establish a clean and renewable photocatalytic hydrogen-production method [6]. The absorption wavelength range of semiconductor materials such as oxides, sulfides, nitrides, and solid solutions was examined under visible light, to improve the absorption wavelength range [7,8].

Heterojunction photocatalysts were used extensively to improve the separation efficiency of photoexcited electron-hole pairs. A single-phase photocatalyst has significant limitations in a photocatalytic response, because photogenerated electrons and holes are quickly mixed [9] to develop optical properties. Jiang et al. doped phosphorus nanosheets with g-C₃N₄ and added carbon defects, which significantly increased the rate of hydrogen evolution through the photocatalytic method [9]. Furthermore, studies report an improved hydrogen production rate through using a mineral acid or phosphoric acid etching of g-C₃N₄ nanosheets to increase the number of active sites [10,11].

Graphite carbon nitride (g-C₃N₄) has recently gained new interest as a promising material in different applications such as photocatalysts, fuel cell electrodes, light-emitting devices, and chemical sensors. g-C₃N₄ stands out amongst many types of photocatalysts. A polymer photocatalyst bandgap is about 2.7 eV, allowing visible light to absorb up to 460 nm. Nevertheless, g-C₃N₄ can absorb visible light effectively since graphitic C₃N₄ has an adequate conduction band under illumination conditions that is able to be more harmful than protons formed by hydrogen [12,13]. Tungsten oxide (WO₃) is considered a promising material [13,14]. It has been reported that synthesis of WO₃/g-C₃N₄ composite organic compounds shapes a heterostructural composite photocatalyst [15,16], provided that the electron donor is an aqueous solution for triethanolamine. In the color-sensitization method, we looked at the composite catalyst's hydrogen production behavior under visible-light irradiation. g-C₃N₄ composite, blended with WO₃ using a planetary mill, was prepared using hydrothermal treatment to improve its photocatalytic activity [15]. The photocatalytic activity incorporated WO₃ in g-C₃N₄ composite organic compounds [17]. J. Liang et al. [18] investigated the use of crystalline phase engineering in WO₃/g-C₃N₄ composite organic compounds to improve photocatalytic activity under visible light. They demonstrated that WO₃/g-C₃N₄ composites with h-WO₃ show better dispersion of WO₃, higher charge separation, and higher photocatalytic activity through visible-light photocatalytic degradation of Rhodamine B (RhB).

In this research, incorporating WO₃ into g-C₃N₄ composite organic compound photocatalysts were prepared, and exhibited improved photocatalytic activity under visible light. Their morphological, diffused reflectance UV-Vis optical, and (Methylene blue (MB) and phenol) photocatalytic activity properties were analyzed and discussed in detail, to understand the effects of WO₃ on g-C₃N₄ composite organic compounds.

2. Experimental Parts

2.1. Regents

In the experiment, an analytical grade of melamine, sodium tungstate dihydrate (Na₂WO₄·2H₂O) ACS reagent, ≥99%, and other chemicals purchased from Sigma-Aldrich were used. These chemicals did not need further purification as they were of analytical grade. De-ionized water was utilized to avoid contamination.

2.2. Synthesis of Pure g-C₃N₄ and WO₃/g-C₃N₄ Composite Organic Compounds

Simple g-C₃N₄ synthesis involves melamine pyrolysis prepared in an air atmosphere. Initially, 8 g of melamine was ground inside a crucible, then heated at a rate of 5 °C per min until it attained 550 °C, and then adjusted at this temperature for 2 h. Afterwards, the samples were left to cool down to ambient temperature. In the mortar, the resultant powder was then ground with a pestle. Following the first stage, Na₂WO₄·2H₂O was added to melamine to synthesize the doped WO₃/g-C₃N₄ composite organic compounds, after which the procedure for pure g-C₃N₄ was repeated.

2.3. Characterization Techniques

The effect of WO₃ on the physical structure of the g-C₃N₄ composite organic compounds for the 13 structures was characterized by X-ray diffraction. Shimadzu X-ray Diffractometer (XRD-6000 Series) was utilized with the standard copper X-ray tube at 30 kV and 30 mA with a wavelength equal to 1.5406 Å. The surface structure of all samples was evaluated by scanning electron microscopy (SEM-JSM6360 Series, with an acceleration voltage = 20 kV).

The effect of WO₃ on g-C₃N₄ nanocomposite organic compounds was tested employing a UV-vis-NIR spectrophotometer model (Shimadzu UV-3600) with diffused reflectance in a wide range between 200 and 800 nm. The device was designed with the BaSO₄ built-in sphere attachment as reference material. To counteract the WO₃/g-C₃N₄ composites within the holder, as a guide for the BaSO₄ and the other holder, a specifically constructed holder attached to the integrating sphere device was employed. The thickness of the holder corresponds to the thickness of the WO₃/g-C₃N₄ nanocomposites. To track the photo-removal phase, a UV-visible spectrophotometer was used.

The diffused reflectance was measured in ambient conditions using a JASCO UV-Vis-NIR-V-570 double beam spectrophotometer.

2.4. Photocatalytic Measurements

A simple wooden photoreactor tested the photocatalytic activity of WO₃/g-C₃N₄ nanocomposites under visible-light spectrum radiation of samples, using both methylene blue (MB) and aqueous phenol as a pollutant example in wastewater. I.S. Yahia and his group designed the photoreactor in NLEBA, Ain Shams University (ASU), Egypt, consisting of two parts: the outer part was in the form of a box made from wood (height: 100 cm, width: 65 cm); the inner part had seven visible lamps (18 W, 60 cm length, 425 to 600 nm), and could be separately controlled. Each set of nanopowders was placed in a beaker containing 50 mL of MB (20 mg/L) (i.e., for the phenol photodegradation). The sample was magnetically stirred in the dark system to reach equilibrium between dye and photocatalyst. The sample was removed from the solution after a specific time (every 15 min), and the amount of sample remaining was then exposed to visible light. A UV-Vis spectrophotometer was used to analyze the samples.

3. Results and Discussions

3.1. Structural XRD Measurements

The crystalline structure phase was analyzed with the XRD technique to reveal the effect of doping WO₃ in the final products. XRD patterns are shown in Figure 1 for pure g-C₃N₄ and its doping with WO₃ on the g-C₃N₄ composite organic compounds, with various WO₃ effects. As visualized in Figure 1, the g-C₃N₄ powder sample highlights two peaks at $2\theta = 13.1^\circ$, and $2\theta = 27.4^\circ$, which can be indexed to a small peak, (100) plane, pertinent to the in-plane structural packing of graphitic material, and a sharp peak, (002) plane, assigned to the interlayer spacing of the conjugated aromatic system. The (002) peak indicates a higher-density packing of the g-C₃N₄ molecules. This corresponds to the characteristic interplanar staking peaks of aromatic systems and the inter-layer structural packing, respectively [19,20]. These results are compared with Mo et al. [21]. The peak at $2\theta = 27.4^\circ$ (JCPDS 87-1526) confirms the formation of hexagonal phase g-

C_3N_4 powders [18,20,21]. The introduction of doping WO_3 on $g-C_3N_4$ composite organic compounds reduces the maximum intensity of peaks. In Figure 1, we notice that only two peaks appear in the entirety of the prepared samples related to pure $g-C_3N_4$ except for the last sample, noted as 0.5 g WO_3 -doped $g-C_3N_4$, showing the other two peaks related to WO_3 . The two peaks related to WO_3 appear at $2\theta = 16.9^\circ$ and 32.51° , related to (101) and (022), according to JCPDS 01-083-0950.

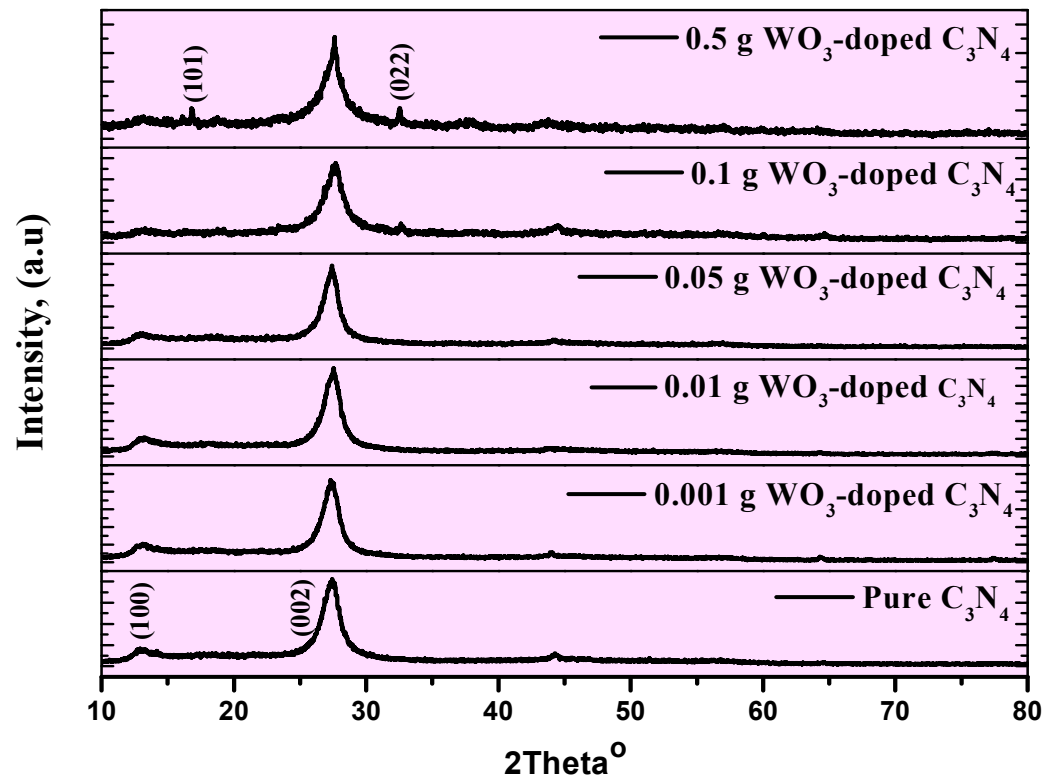


Figure 1. XRD patterns of pure $g-C_3N_4$ powder and its WO_3 doping on $g-C_3N_4$ composite organic compounds (0.001, 0.01, 0.05, 0.1, and 0.5 g of WO_3).

The average crystallite size for the prepared samples was measured using the Debye–Scherrer formula, as follows [22]:

$$D = 0.94\lambda / \beta \cos \theta \quad (1)$$

The calculated crystallite size D depends on the broadening diffraction peak β , the diffraction angle θ , and the X-ray wavelength λ . Both dislocation density δ and lattice strain ε were calculated using the following equations [23,24]:

$$\delta = n/D^2 \quad (2)$$

$$\varepsilon = \beta \cos \theta / 4 \quad (3)$$

The XRD structural parameters for the prepared samples summarized in Table 1 show that the average crystallite size for the pure $g-C_3N_4$ is 39.17 nm, and this increases from 35.91, 35.93, 40.84, 44.83, to 81.67 nm for the 0.5, 0.1, 0.05, 0.01, and 0.001 WO_3 -doped $g-C_3N_4$ composites, respectively.

The lower dislocation density values reflect the higher quality of the prepared samples.

Table 1. N_4 and its $WO_3/g-C_3N_4$ with various amounts of tungsten oxide (0.001, 0.01, 0.05, 0.1, and 0.5% WO_3).

| Samples | Phases | Mean Values | | |
|----------------------------------|--------------------------|------------------------|-------------------------------------|------------------------|
| | | Crystallite Size, (nm) | Dislocation Density, ($1/(nm)^2$) | Lattice Strain |
| Pure $g-C_3N_4$ | Pure $g-C_3N_4$ | 39.17 | 6.51×10^{-4} | 8.850×10^{-4} |
| 0.001 g WO_3 -doped $g-C_3N_4$ | Pure $g-C_3N_4$ | 35.91 | 7.999×10^{-4} | 9.753×10^{-4} |
| 0.01 g WO_3 -doped $g-C_3N_4$ | Pure $g-C_3N_4$ | 35.93 | 7.993×10^{-4} | 9.749×10^{-4} |
| 0.05 g WO_3 -doped $g-C_3N_4$ | Pure $g-C_3N_4$ | 40.84 | 6.866×10^{-4} | 8.886×10^{-4} |
| 0.1 g WO_3 -doped $g-C_3N_4$ | Pure $g-C_3N_4$ | 44.83 | 9.336×10^{-4} | 9.667×10^{-4} |
| 0.5 g WO_3 -doped $g-C_3N_4$ | Phase 1: Pure $g-C_3N_4$ | 81.76 | 1.710×10^{-4} | 4.436×10^{-4} |
| | Phase 2: WO_3 | 52.93 | 3.641×10^{-4} | 6.593×10^{-4} |

3.2. Morphologies and Microstructure Analysis

To assess the effect of WO_3 in $g-C_3N_4$ composite organic photocatalyst compounds, the morphology and microstructure of the pure $g-C_3N_4$ and its WO_3 -doped $g-C_3N_4$ composite organic compounds was studied by using SEM image analysis. Figure 2a–f presents the SEM images of the investigated composite photocatalysts. The morphology of pure $g-C_3N_4$ exhibited apparent granular aggregates and a typical sheet that consisted of small particles created from some irregular particles. Figure 2c–f shows that the WO_3 particles were attached to the surface of the sheet $g-C_3N_4$. The particle sizes obtained from SEM images of the investigated composite organic compounds were gathered in Table 2. The particle sizes varied between 1.65 and 1.51 μm . As the WO_3 doping particle contents increased, the $g-C_3N_4$ composite photocatalyst had no noticeable influence on the obtained particle size. A similar result is reported by X. Chu et al. [25].

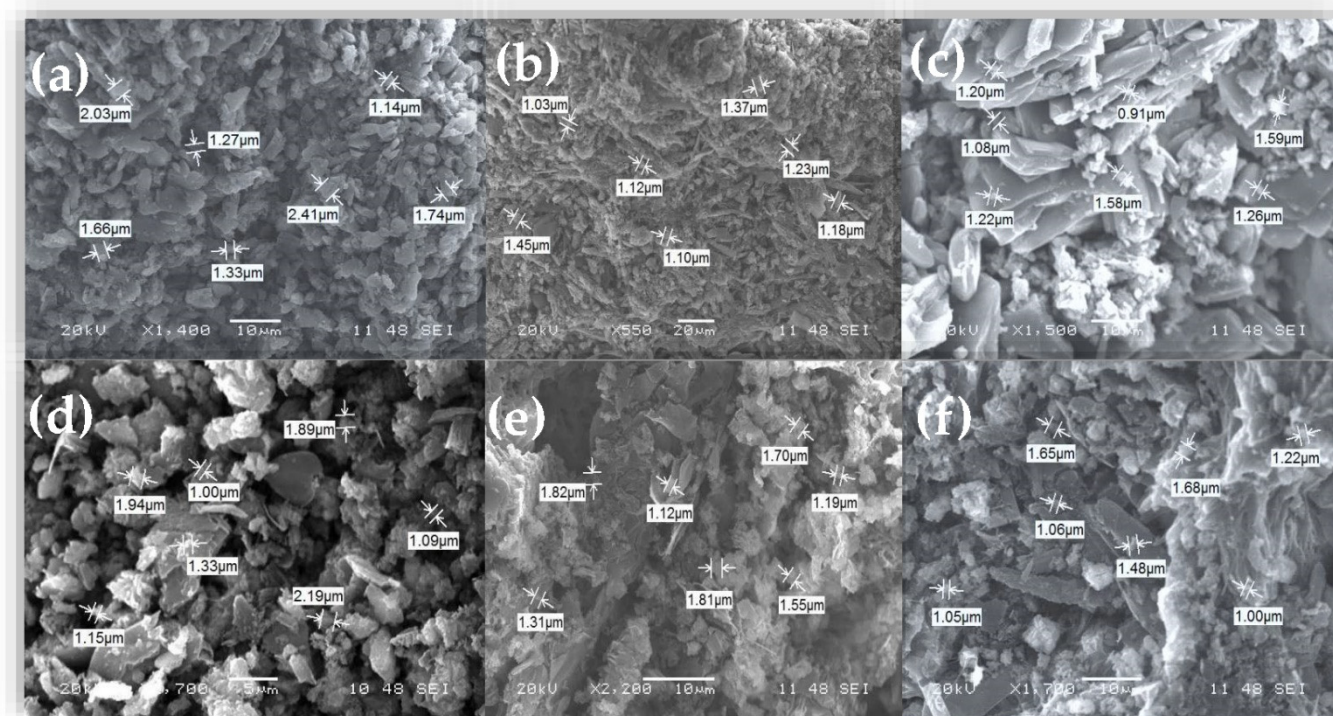
**Figure 2.** (a–f) SEM images of pure $g-C_3N_4$ and its $WO_3/g-C_3N_4$ nanocomposite organic compounds with various amounts of tungsten oxide (0.001, 0.01, 0.05, 0.1, and 0.5 g of WO_3 , respectively).

Table 2. Particle size and corresponding rate constants of pure g-C₃N₄ and its WO₃/g-C₃N₄, with various amounts of tungsten oxide (0.001, 0.01, 0.05, 0.1, and 0.5% WO₃).

| Samples | Particle Size, (μm) | K, (min ⁻¹) | |
|--|---------------------|-------------------------|--------|
| | | MB | Phenol |
| Pure g-C ₃ N ₄ | 1.65 | 0.0028 | 0.0053 |
| 0.001 g WO ₃ /g-C ₃ N ₄ | 1.21 | 0.0054 | 0.0064 |
| 0.01 g WO ₃ /g-C ₃ N ₄ | 1.26 | 0.0049 | 0.0092 |
| 0.05 g WO ₃ /g-C ₃ N ₄ | 1.3 | 0.0108 | 0.0194 |
| 0.1 g WO ₃ /g-C ₃ N ₄ | 1.5 | 0.0052 | 0.0172 |
| 0.5 g WO ₃ /g-C ₃ N ₄ | 1.51 | 0.0045 | 0.0145 |

3.3. Optical Properties of WO₃ Doped g-C₃N₄ Nanocomposites

Figure 3a shows the optical UV-Vis diffused reflectance spectroscopy study to identify the bandgap energy of pure g-C₃N₄ and WO₃-doped g-C₃N₄ composite organic photocatalyst compounds. The optical UV-Vis diffused reflectance spectra for other WO₃/g-C₃N₄ photocatalyst composite samples should be the superimposed signals of g-C₃N₄. All diffused reflection spectra increased with increasing wavelengths up to 400 nm. The absorption edge spectra start to redshift towards the visible region, allocated to the intrinsic g-C₃N₄ bandgap [25].

The redshift suggested that the photocatalyst composite compounds could use sunlight and produce more electron-hole pairs, which would help the photocatalytic response. The above findings may be caused by the interactions between the WO₃ and g-C₃N₄ incorporated into the heterojunction materials. Figure 3b,c displays the direct and indirect energy bandgap of pure g-C₃N₄ and its WO₃ atom-doped g-C₃N₄ composite organic photocatalyst compounds, which can be estimated from the plots of $(\alpha hv)^2$ and $(\alpha hv)^{1/2}$ vs. the incident photon energy (hv) using Tauc's formula [26]. The Kubelka–Munk function and its related absorption coefficient (α) are as follows [27–29]:

$$A hv = (F(R) hv/d) = A(hv - E_g)^r \quad (4)$$

where A is a pre-factor, E_g is the energy bandgap, and r limits the transition band type. When $r = 2$ is related to the indirect allowed band, $r = 1/2$ is associated with the direct allowed band. The bandgap of the photocatalyst was determined by Tauc's plot, where $(\alpha hv)^{1/2}$ with hv axis (i.e., the linear portion of the plots $(\alpha hv)^2$ with hv axis). By drawing a tangent line of each curve, each photocatalyst composite material's bandgap was obtained from the intercept hv axis. Therefore, the estimated bandgaps of pure g-C₃N₄ and its WO₃ atom-doped g-C₃N₄ composite organic photocatalyst compounds, with various WO₃ content, confirmed that the direct and indirect bandgaps for g-C₃N₄ were 2.83 [30] and 2.56 eV, respectively. This result was also reported by J.Y. Tai et al. [31]. For the indirect bandgap, we noted a slight change from 2.56 eV for the pure g-C₃N₄ changing to 2.6, 2.65, 2.66, 2.86, to 2.71 eV for the 0.5, 0.1, 0.05, 0.01, and 0.001 WO₃-doped g-C₃N₄ composite, respectively. For the direct bandgap, a small change was also noted, from 2.83 eV for the pure g-C₃N₄ changing to 2.86, 2.88, 2.89, 2.90, 2.92 eV for the 0.5, 0.1, 0.05, 0.01, and 0.001 WO₃-doped g-C₃N₄ composite, respectively. This indicated that the increase in WO₃ content in the composite photocatalyst had no evident influence on bandgap energy. However, it was found that the movement and lifetime of the photogenerated charge carriers in g-C₃N₄ could be significantly affected by such a combination.

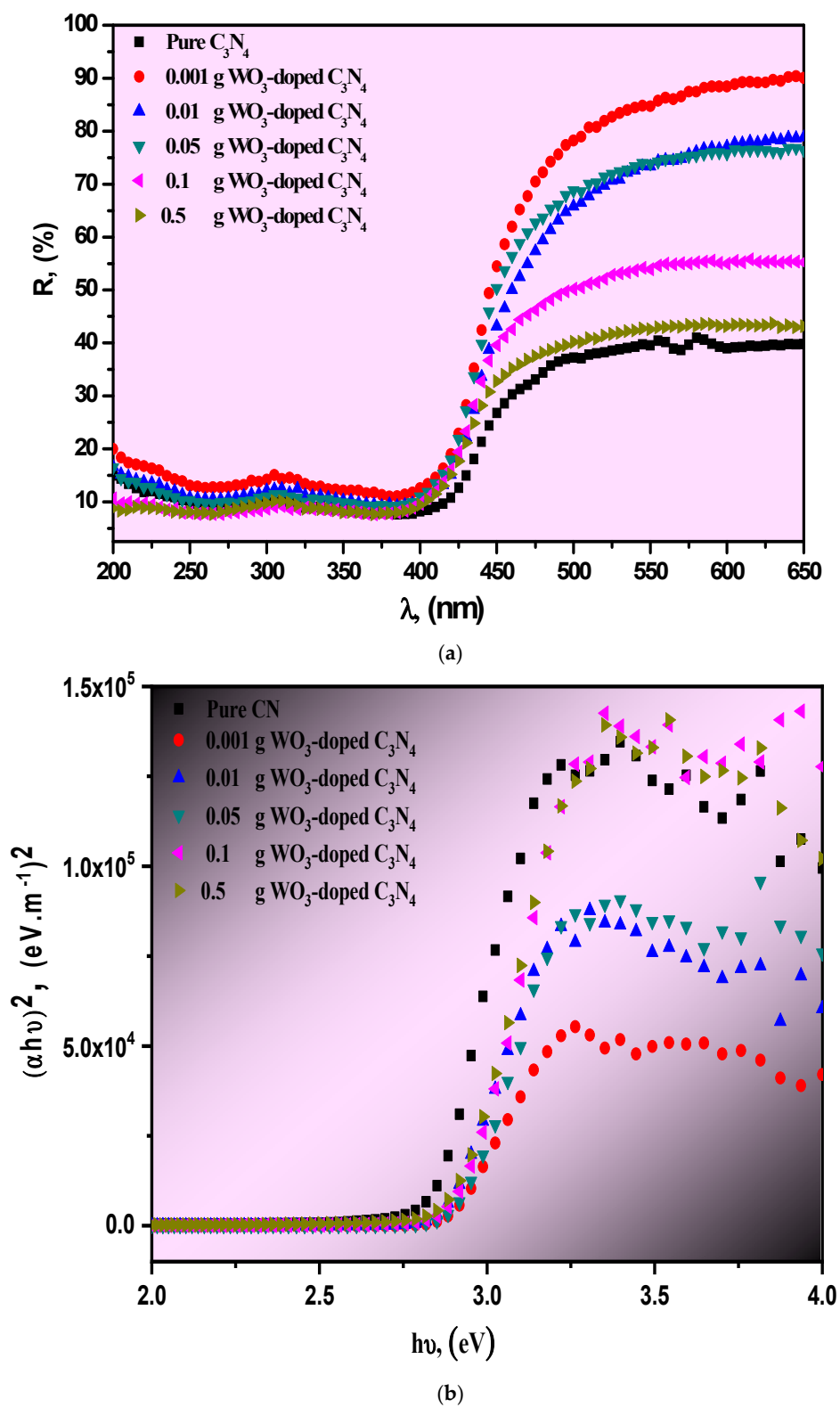


Figure 3. Cont.

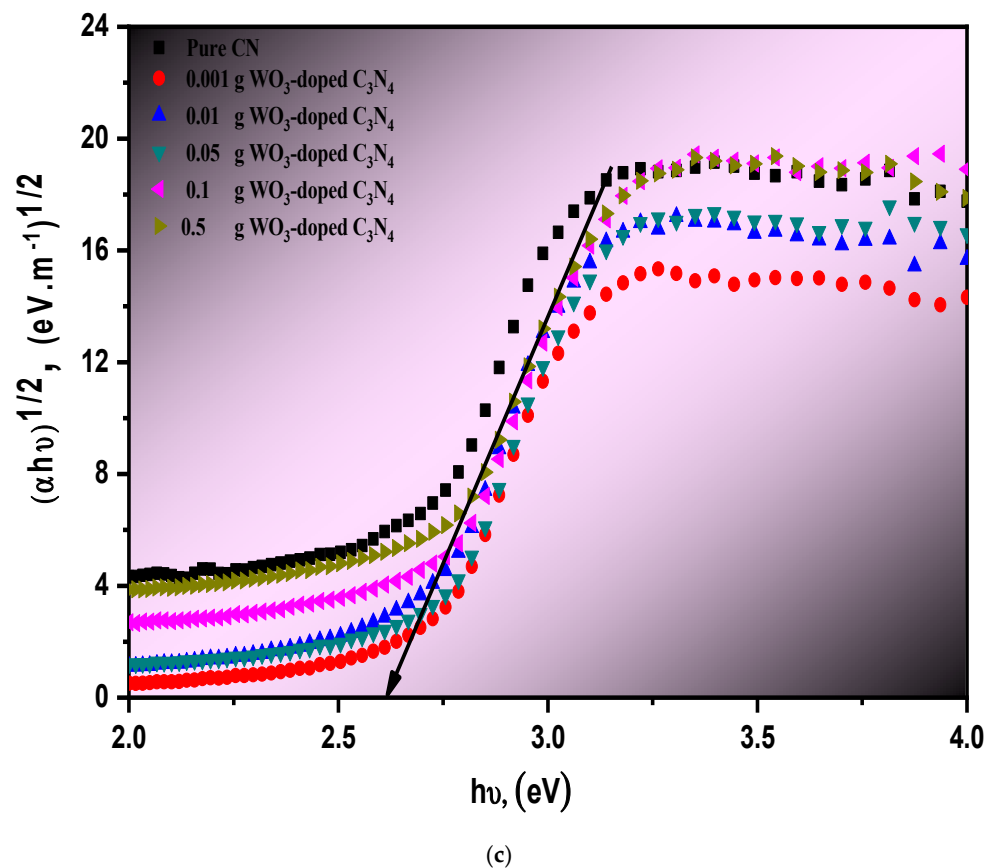


Figure 3. (a–c) Diffused reflectance optics UV-Vis (a), $(\alpha h\nu)^2$ (b) and $(\alpha h\nu)^{1/2}$ (c) versus the incident photon energy $h\nu$ of pure $g\text{-C}_3\text{N}_4$ and its $\text{WO}_3/g\text{-C}_3\text{N}_4$, with various amounts of tungsten oxide (0.001, 0.01, 0.05, 0.1, and 0.5 g of WO_3).

3.4. Kinetics of the Photodegradation Process of WO_3 -Doped $g\text{-C}_3\text{N}_4$ Nanocomposites

The photocatalytic performances of pure $g\text{-C}_3\text{N}_4$ and its $\text{WO}_3/g\text{-C}_3\text{N}_4$ composites, with various concentrations, were assessed using MB and phenol contaminants under visible-light irradiation. The extent of the concentration of MB and phenol contaminants on the photocatalyst was measured in the dark system until equilibrium. The equilibrium between the prepared photocatalyst and the investigated organic pollutants, MB, as a colored dye, and phenol, as a colorless organic compound, was recognized after 30 min of stirring. The photocatalytic performances of pure $g\text{-C}_3\text{N}_4$ and its $\text{WO}_3/g\text{-C}_3\text{N}_4$ composites with different photocatalysts were investigated for the photodegradation of MB and phenol contaminants. The achieved results are shown in Figure 4a,b. Figure 4a shows a limited photocatalytic performance of the pure $g\text{-C}_3\text{N}_4$ toward MB. However, the improved photocatalytic performance of $\text{WO}_3/g\text{-C}_3\text{N}_4$ composites was recorded, indicating a major effect on the photocatalytic activity of $g\text{-C}_3\text{N}_4$ when modified with WO_3 . In general, the composite's photocatalytic activity increased after WO_3 was applied, and enhanced photocatalytic activity of 0.05% WO_3 was noted.

Nevertheless, the increase in WO_3 (0.1 and 0.5) has been found to reduce photocatalytic efficiency, which may be due to the decrease in visible-light absorption catalytic sites. Additionally, the same behavior was observed for the degradation of phenol. The composite material containing 0.5% WO_3 showed the maximum performance for phenol degradation, which can be attributed to the production of the WO_3 -semiconductor heterojunction effectively, which leads to transfer of charge from $g\text{-C}_3\text{N}_4$ under the visible-light irradiation. Moreover, the kinetics of the degradation of MB and phenol was noticed to follow the pseudo-first-order model, and the reaction rates were calculated by Equation (2) [32]:

$$\ln(C_0/C) = Kt, \tag{5}$$

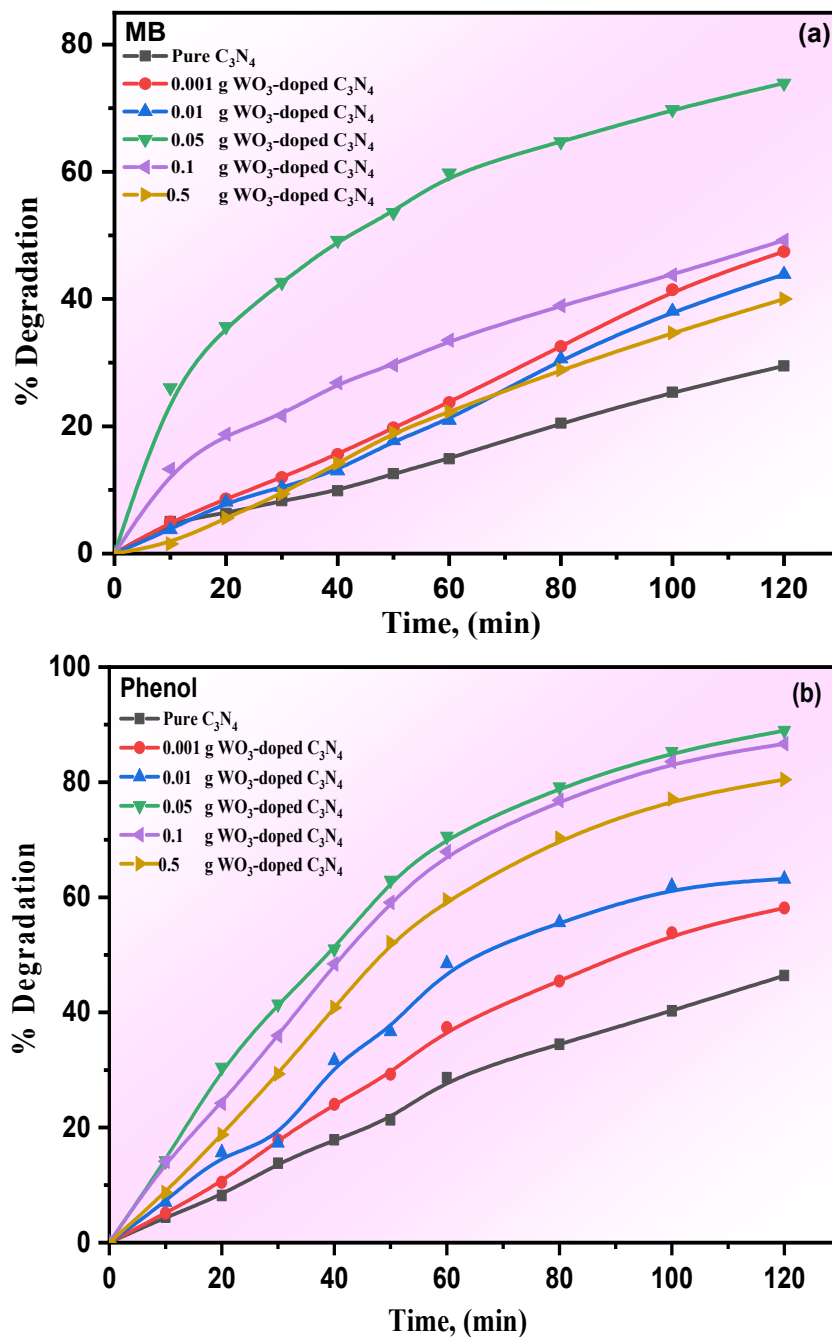


Figure 4. The degradation (%) of MB (a,b) phenol for pure g-C₃N₄ and its WO₃/g-C₃N₄ nanocomposites.

Here, C_0 and C are the concentrations at the initial step and regular time intervals, respectively. Additionally, K is the pseudo-first-order reaction-rate constant (min^{-1}) for investigated organic contaminants, and t is the time (min). Figure 5a,b shows the linear relationship between $\ln(C_0/C)$ and t . According to these results, the photodegradation of MB and phenol pollutants follows pseudo-first-order reaction kinetics. Additionally, the degradation rate relies on the concentration of the organic substrate. Figure 6 shows the constant rate values for the degradation of MB and phenol contaminants. Percentage of degradation can be calculated to determine the efficiency of the prepared catalysts in the photocatalytic reaction, as illustrated in Figure 5. The efficiency of degradation

increases with WO_3 content to 0.5%, then the efficiency decreases. It can be noted that the photocatalytic degradation rates of MB had better rate-constant characteristics than the photocatalytic degradation rates of phenol. The photodegradation using MB and phenol contaminants in aqueous solution improvement onto pure $g-C_3N_4$ and its $WO_3/g-C_3N_4$ photocatalyst composites with various concentrations was evaluated under visible light. Dependant on variations in the WO_3 content, the plot of the irradiation time (t) against $-\ln(C/C_0)$ was nearly a straight line. This result has also been reported by G. Lui et al. [33]. The corresponding estimated degradation rate constants (K) were added to Table 2.

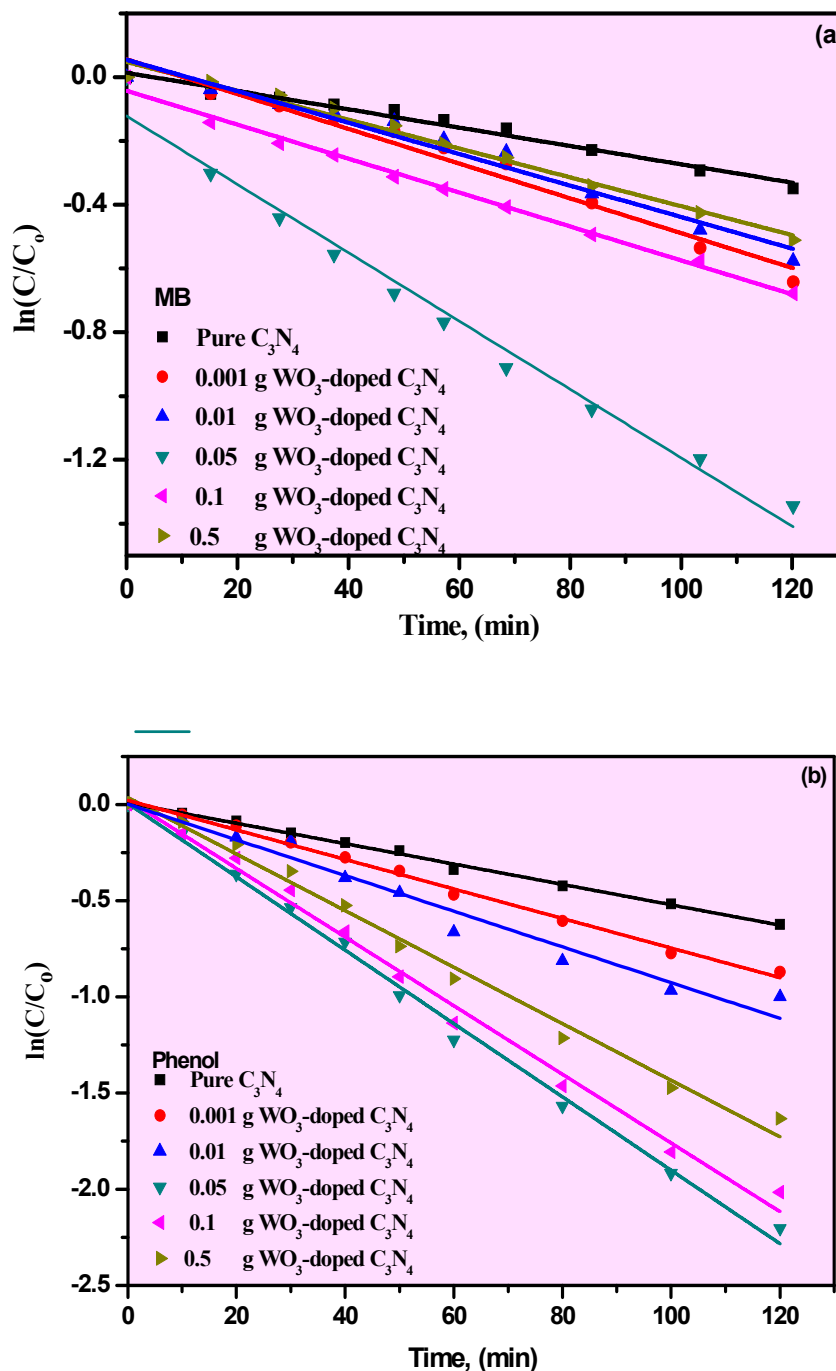


Figure 5. (a,b) The kinetic degradation curves of MB (a) and (b) Phenol for pure $g-C_3N_4$ and its $WO_3/g-C_3N_4$ nanocomposites.

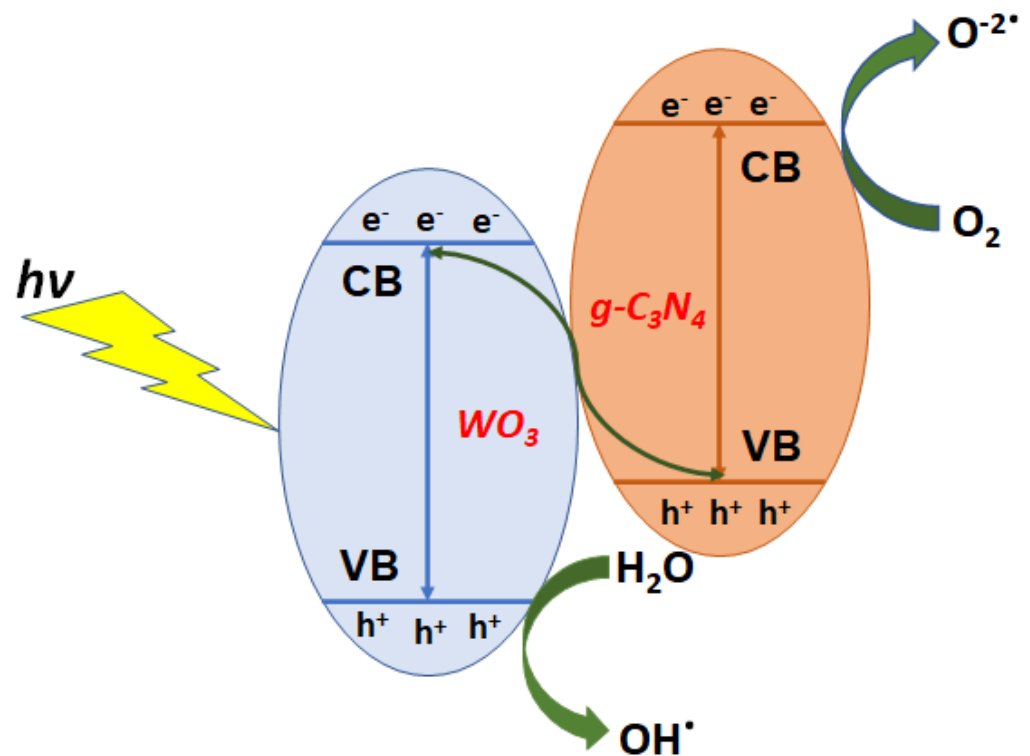
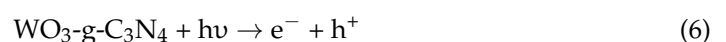


Figure 6. Photocatalytic mechanism of $\text{WO}_3/\text{g-C}_3\text{N}_4$ nanocomposites.

3.5. Photodegradation Conduction Mechanism of WO_3 -Doped $\text{g-C}_3\text{N}_4$ Nanocomposites

The proposed mechanism for photocatalytic behavior of $\text{WO}_3/\text{g-CN}$ composite under the visible spectrum is interpreted in Figure 6. It is a successfully designed $\text{WO}_3/\text{g-CN}$ composite with various WO_3 . The Kubelka–Munk method was used to calculate the valence band (VB) and conduction band (CB) edge potentials of the prepared pure g-CN and $\text{WO}_3/\text{g-CN}$ with different concentrations of WO_3 . The direct and indirect bandgaps for g-CN are 2.83 and 2.56 eV, respectively. The increase in WO_3 content in the $\text{WO}_3/\text{g-CN}$ composite significantly influences bandgap energy [34]. The proposed system suggests that both g-CN and WO_3 will likely offer photogenerated charge carriers. The photogenerated electron in CB of WO_3 then flows to VB of $\text{g-C}_3\text{N}_4$ due to electrostatic forces of attraction between the electron in CB of WO_3 and the hole in VB g-CN , reducing the recombination of electrons and holes in the $\text{WO}_3/\text{g-C}_3\text{N}_4$ composite and assisting in enhancing the charge separation spatially.

Furthermore, the electrons in the CB of $\text{g-C}_3\text{N}_4$ can also be retained by reducing the molecular oxygen O_2 to form $\text{O}^{-2\bullet}$, due to the negative nature of the CB edge potential compared to the standard redox capability of $\text{O}_2/\text{O}^{-2\bullet}$ [35]. Thus, the hole created in the VB of WO_3 leads interacts with H_2O to generate OH^\bullet radicals, giving the more positive potential of the VB than the standard redox capability of OH/OH^- . In this manner, the production of $\text{O}^{-2\bullet}$ and OH^\bullet radicals plays a significant role in the photodegradation of MB and phenol degradation under visible light. With both OH^\bullet and O^{-2} , the phenol and Methylene Blue dyes produced CO_2 and H_2O [36,37].



In comparison to the previous work, our 0.5% WO₃/g-C₃N₄ has the highest photocatalytic activity of both MB and phenol in the presence of visible light, as shown in Table 3. Using the hydrothermal impregnation and calcination method, Cong Zhao et al. [38] obtained simple and inexpensive C-doped g-C₃N₄/WO₃ as highly active photocatalysts. Tao Pan et al. [39] prepared WO₃/g-C₃N₄ that showed improved photocatalytic activity for TC degradation. Perhaps most importantly, the UV-C-induced-TC degradation activity outperformed all other degradations regardless of concentration or pH level. According to Zhao et al. [40], the Ag/WO_{2.9}/g-C₃N₄ composite outperforms pure g-C₃N₄ and pure WO₃ in terms of light-selective adsorption and photocatalysis. Hong Yan et al. [41] proved that WO₃/g-C₃N₄-modified nanocomposites had more significant photocatalytic activity than pure WO₃ and pure g-C₃N₄. Junling Zhao et al. [19] discovered that WO₃/g-C₃N₄ photocatalysts have increased degradation activities towards RhB dye when exposed to simulated sunlight. Minji Yoon et al. [42] demonstrated that WO₃/g-C₃N₄ does not exhibit any photocatalytic activity on the degradation of p-nitrophenol. On the other hand, the degradation rate of p-nitrophenol was remarkably increased by the addition of Fenton to WO₃/g-C₃N₄, which means that photocatalytic activity was further enhanced in the presence of hydrogen peroxide (H₂O₂) because of the generation of hydroxyl radicals.

Table 3. Photocatalytic comparison between the prepared WO₃/g-C₃N₄ and various previous works.

| Photocatalyst | Method of Preparation | Organic Solution | Irradiation Time | Source | % Degradation | Refs. |
|--|---------------------------|------------------|------------------|--------------------|---------------|--------------|
| WO ₃ /g-CN | Pyrolysis | MB Phenol | 120 min | Visible Light lamp | 80% 90% | Present work |
| C-doped g-C ₃ N ₄ /WO ₃ | Hydrothermal impregnation | Tetracycline | 60 min | UV-light lamp | 75% | [33] |
| WO ₃ /g-C ₃ N ₄ | Calcination method | Tetracycline | 120 min | Xenon lamp | 90.54% | [34] |
| Ag/WO ₃ /g-C ₃ N ₄ | Calcination method | MB | 300 min | UV-light lamp | — | [35] |
| WO ₃ /g-C ₃ N ₄ | Thermal polymerization | MO | 120 min | Xenon lamp | 93% | [36] |
| WO ₃ /g-C ₃ N ₄ | Hydrothermal | RhB | 90 min | UV-light lamp | 91% | [37] |
| WO ₃ /g-C ₃ N ₄ /Photo-Fenton | Calcination method | P-nitrophenol | 240 min | Xenon lamp | 91% | [38] |

3.6. Recycling of WO₃-Doped g-C₃N₄ Nanocomposites

A 0.05 WO₃/g-CN was subjected re-use in photodegradation of MB and phenol for 4 cycles. Figure 7 represents the recycling and reusability of WO₃/g-C₃N₄. The samples exhibited high performance without further decreased reaction rate, which means that WO₃/g-C₃N₄ is a promising material in MB and phenolic compound photodegradation.

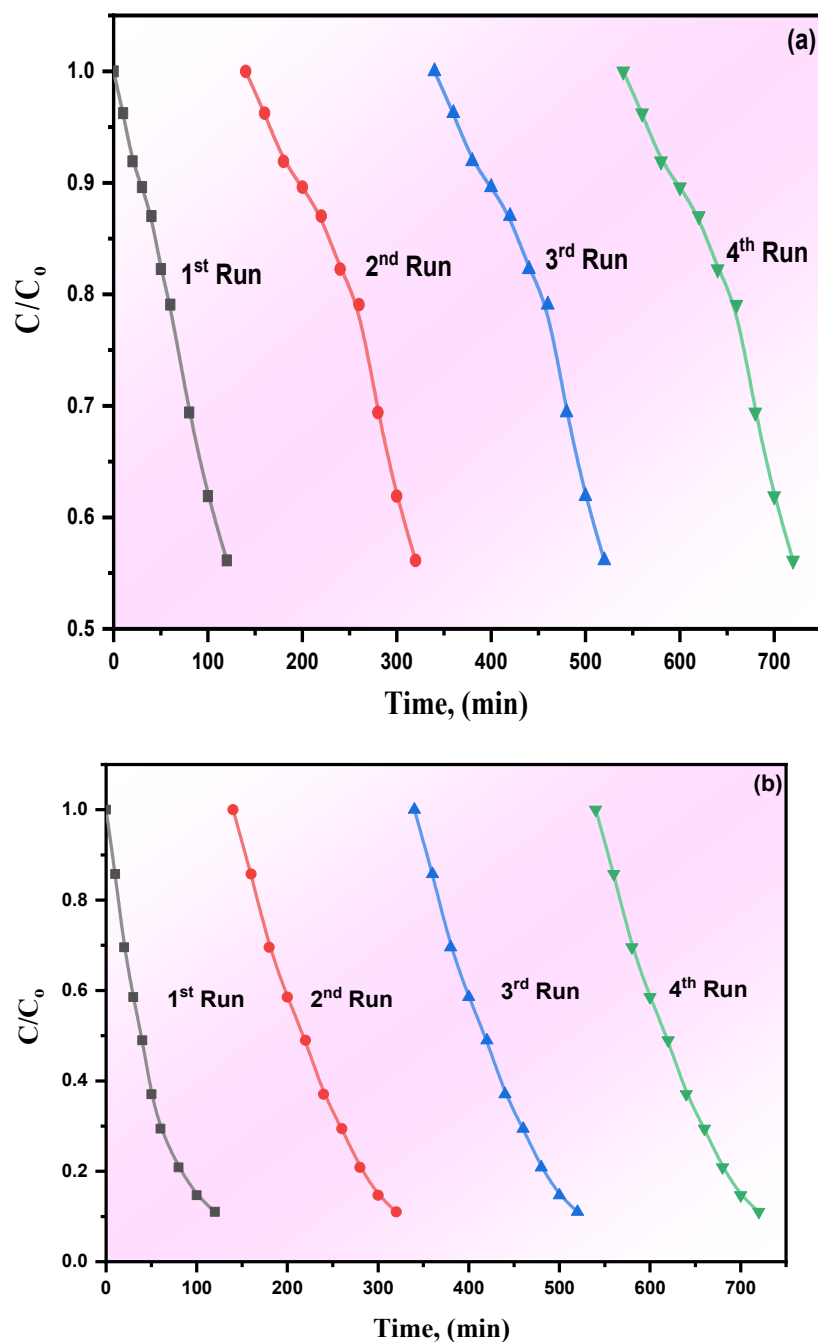


Figure 7. The recycling process for pure $g-C_3N_4$ and its $WO_3/g-C_3N_4$ nanocomposites in photodegradation of (a) MB, (b) phenol.

4. Conclusions

Novel, efficient $WO_3/g-C_3N_4$ nanocomposite with various concentrations of graphitic carbon nitride ($g-C_3N_4$) was prepared. The prepared composites exhibited improved photocatalytic activity on the degradation of MB and phenol under visible-light irradiation. The composite material containing 0.5% WO_3 showed the maximum MB and phenol degradation performance. The kinetic study showed that the pseudo-first-order kinetic best fitted the photocatalytic process. A mechanism was proposed to degrade organic pollutants using $WO_3/g-C_3N_4$ composites under visible-light irradiation.

Author Contributions: Conceptualization, I.S.Y., M.S.A.H. and M.A.I.; methodology, M.S.A.H., A.B., H.S.M.A.-R. and H.Y.Z.; investigation, M.S.A.-w., W.A., N.S.A. and I.S.Y.; resources, I.S.Y. and M.S.A.H.; data curation, M.S.A.-w., W.A., N.S.A. and I.S.Y.; writing—original draft preparation, M.S.A.-w., M.S.A.H. and H.Y.Z.; supervision, I.S.Y., M.A.I., and N.S.A.; funding acquisition, M.S.A.-w. and I.S.Y. All authors have read and agreed to the published version of the manuscript.

Funding: The authors express their appreciation to the Deputyship for Research and Innovation, Ministry of Education, in Saudi Arabia, for funding this research work through the project number: (IFP-KKU-2020/10).

Institutional Review Board Statement: Not applicable.

Informed Consent Statement: Not applicable.

Data Availability Statement: The data supporting this study's findings are available from the corresponding author upon reasonable request.

Conflicts of Interest: The authors declare no conflict of interest.

References

1. Ngullie, R.C.; Alaswad, S.O.; Bhuvanewari, K.; Shanmugam, P.; Pazhanivel, T.; Arunachalam, P. Synthesis and characterization of efficient ZnO/g-C₃N₄ nanocomposites photocatalyst for Photocatalytic degradation of methylene blue. *Coatings* **2020**, *10*, 500. [[CrossRef](#)]
2. Ismael, M.; Elhadad, E.; Wark, M. Construction of SnO₂/g-C₃N₄ composite photocatalyst with enhanced interfacial charge separation and high efficiency for hydrogen production and Rhodamine B degradation. *Colloids Surf. A Physicochem. Eng. Asp.* **2022**, *638*, 128288. [[CrossRef](#)]
3. Wei, H.; Zhang, Y.; Zhang, Y.; Zhang, Y. Design and synthesis of a new high-efficiency CeO₂/SnS₂/polyaniline ternary composite visible-light photocatalyst. *Colloid Interface Sci. Commun.* **2021**, *45*, 100550. [[CrossRef](#)]
4. Moniz, S.J.A.; Shevlin, S.A.; Martin, D.J.; Guo, Z.X.; Tang, J. Visible-light driven heterojunction photocatalysts for water splitting—a critical review. *Adv. Funct. Mater.* **2015**, *8*, 2421–2440. [[CrossRef](#)]
5. Kudo, A.; Miseki, Y. Heterogeneous photocatalyst materials for water splitting. *Chem. Soc. Rev.* **2008**, *48*, 1685–1687. [[CrossRef](#)]
6. Hisatomi, T.; Kubota, J.; Domen, K. Recent advances in semiconductors for photocatalytic and photoelectrochemical water splitting. *Chem. Soc. Rev.* **2014**, *43*, 7520. [[CrossRef](#)]
7. Chen, X.; Shangguan, W. Hydrogen production from water splitting on CdS-based photocatalysts using solar light. *Front. Energy* **2013**, *7*, 111–118. [[CrossRef](#)]
8. Honda, K. One and Two-dimensional Structure of Alpha-Helix and Beta-Sheet Forms of Poly(L-Alanine) shown by Specific Heat Measurements at Low Temperatures (1.5–20 K), 1910.
9. Kong, L.; Jiang, Z.; Lai, H.H.; Nicholls, R.J.; Xiao, T.; Jones, M.O.; Edwards, P.P. Unusual reactivity of visible-light-responsive AgBr–BiOBr heterojunction photocatalysts. *J. Catal.* **2012**, *293*, 116–125. [[CrossRef](#)]
10. Gao, Y.; Hou, F.; Hu, S.; Wu, B.; Wang, Y.; Zhang, H.; Jiang, B.; Fu, H. Graphene quantum-dot-modified hexagonal tubular carbon nitride for visible-light photocatalytic hydrogen evolution. *ChemCatChem* **2018**, *10*, 1330–1335. [[CrossRef](#)]
11. Ding, C.; Shi, J.; Wang, Z.; Li, C. Photoelectrocatalytic water splitting: Significance of cocatalysts, Electrolyte, and Interfaces. *ACS Catal.* **2017**, *7*, 675–688. [[CrossRef](#)]
12. Xing, P.; Zhou, F.; Li, Z. Preparation of WO₃/g-C₃N₄ composites with enhanced photocatalytic hydrogen production performance. *Appl. Phys. A* **2019**, *125*, 788. [[CrossRef](#)]
13. Nakajima, T.; Kitamura, T.; Tsuchiya, T. Visible light photocatalytic activity enhancement for water purification in Cu(II)-grafted WO₃ thin films grown by photoreaction of nanoparticles. *Appl. Catal. B Environ.* **2011**, *108–109*, 47–53. [[CrossRef](#)]
14. Tong, T.; Zhu, B.; Jiang, C.; Cheng, B.; Yu, J. Mechanistic insight into the enhanced photocatalytic activity of single-atom Pt, Pd or Au-embedded g-C₃N₄. *Appl. Surf. Sci.* **2018**, *433*, 1175–1183. [[CrossRef](#)]
15. Li, Z.; Ma, Y.; Hu, X.; Liu, E.; Fan, J. Enhanced photocatalytic H₂ production over dual-cocatalyst-modified g-C₃N₄ heterojunctions. *Chin. J. Catal.* **2019**, *40*, 434–445. [[CrossRef](#)]
16. Kim, J.; Lee, C.W.; Choi, W. Platinized WO₃ as an environmental photocatalyst that generates OH radicals under visible light. *Environ. Sci. Technol.* **2010**, *44*, 6849–6854. [[CrossRef](#)]
17. Jin, Z.; Murakami, N.; Tsubota, T.; Ohno, T. Complete oxidation of acetaldehyde over a composite photocatalyst of graphitic carbon nitride and tungsten(VI) oxide under visible-light irradiation. *Appl. Catal. B Environ.* **2014**, *150–151*, 479–485. [[CrossRef](#)]
18. Liang, J.; Li, Y.; Zhang, J.; Li, C.; Yang, X.; Chen, X.; Wang, F.; Chen, C. Crystalline phase engineering in WO₃/g-C₃N₄ composites for improved photocatalytic performance under visible light. *Mater. Res. Express.* **2020**, *7*, 065503. [[CrossRef](#)]
19. Zhao, J.; Ji, Z.; Shen, X.; Zhou, H.; Ma, L. Facile synthesis of WO₃ nanorods/g-C₃N₄ composites with enhanced photocatalytic activity. *Ceram. Int.* **2015**, *41*, 5600–5606. [[CrossRef](#)]
20. Wang, X.; Maeda, K.; Thomas, A.; Takanabe, K.; Xin, G.; Carlsson, J.M.; Domen, K.; Antonietti, M. A metal-free polymeric photocatalyst for hydrogen production from water under visible light. *Nat. Mater.* **2008**, *8*, 76–80. [[CrossRef](#)]

21. Wang, S.; Li, Y.; Wang, X.; Zi, G.; Zhou, C.; Liu, B.; Liu, G.; Wang, L.; Huang, W. One-step supramolecular preorganization constructed crinkly graphitic carbon nitride nanosheets with enhanced photocatalytic activity. *J. Mater. Sci. Technol.* **2022**, *104*, 155–162. [[CrossRef](#)]
22. Ansari, A.R.; Hammad, A.H.; Abdel-wahab, M.S.; Shariq, M.; Imran, M. Structural, optical and photoluminescence investigations of nanocrystalline CuO thin films at different microwave powers. *Opt. Quantum Electron.* **2020**, *52*, 1–16. [[CrossRef](#)]
23. Hammad, A.H.; Abdel-wahab, M.S.; Vattamkandathil, S.; Ansari, A.R. Influence the oxygen flow rate on the film thickness, structural, optical and photoluminescence behavior of DC sputtered NiOx thin films. *Phys. B Condens. Matter* **2019**, *568*, 6–12. [[CrossRef](#)]
24. Alzahrani, A.O.M.; Abdel-wahab, M.S.; Alayash, M.; Aida, M.S. Effect of ZnO layer thickness upon optoelectrical properties of NiO/ZnO heterojunction prepared at room temperature. *J. Mater. Sci. Mater. Electron.* **2018**, *29*, 16317–16324. [[CrossRef](#)]
25. Mo, Z.; She, X.; Li, Y.; Liu, L.; Huang, L.; Chen, Z.; Zhang, Q.; Xu, H.; Li, H. Synthesis of g-C₃N₄ at different temperatures for superior visible/UV photocatalytic performance and photoelectrochemical sensing of MB solution†. *RSC Adv.* **2015**, *123*, 101552–101562. [[CrossRef](#)]
26. Kadi, M.W.; Mohamed, R.M. Increasing visible light water splitting efficiency through synthesis route and charge separation in mesoporous g-C₃N₄ decorated with WO₃ nanoparticles. *Ceram. Int.* **2019**, *45*, 3886–3893. [[CrossRef](#)]
27. Tauc, J.; Grigorovici, R.; Vancu, A. Optical properties and electronic structure of amorphous germanium. *Phys. Status Solidi* **1996**, *15*, 627–637. [[CrossRef](#)]
28. Chu, X.; Liu, J.; Liang, S.; Bai, L.; Dong, Y.; Epifani, M. Facile preparation of g-C₃N₄-WO₃ composite gas sensing materials with enhanced gas sensing selectivity to acetone. *J. Sens.* **2019**, *2019*, 6074046. [[CrossRef](#)]
29. Liu, Z.X.; Wang, X.L.; Hu, A.P.; Tang, Q.L.; Xu, Y.L.; Chen, X.H. 3D Se-doped NiCoP nanoarrays on carbon cloth for efficient alkaline hydrogen evolution. *J. Cent. South Univ.* **2021**, *28*, 2345–2359. [[CrossRef](#)]
30. Huang, L.; Xu, H.; Li, Y.; Li, H.; Cheng, X.; Xia, J.; Xu, Y.; Cai, G. Visible-light-induced WO₃/g-C₃N₄ composites with enhanced photocatalytic activity. *Dalton Trans.* **2013**, *42*, 8606. [[CrossRef](#)]
31. Tai, J.Y.; Leong, K.H.; Saravanan, P.; Sim, L.C. Bioinspired Synthesis of Carbon Dots/g-C₃N₄ Nanocomposites for Photocatalytic Application. *E3S Web Conf.* **2018**, *65*, 05015. [[CrossRef](#)]
32. Abdel-wahab, M.S. Substrate temperature impact on the structural, optical and photo-catalytic activity of sputtered Cu-Doped ZnO thin films. *J. Electron. Mater.* **2021**, *50*, 4364–4372. [[CrossRef](#)]
33. Liu, G.; Han, J.; Zhou, X.; Huang, L.; Zhang, F.; Wang, X.; Ding, C.; Zheng, X.; Han, H.; Li, C. Enhancement of visible-light-driven O₂ evolution from water oxidation on WO₃ treated with hydrogen. *J. Catal.* **2013**, *307*, 148–152. [[CrossRef](#)]
34. Sun, X.Y.; Zhang, F.J.; Kong, C. Porous g-C₃N₄/WO₃ photocatalyst prepared by simple calcination for efficient hydrogen generation under visible light. *Colloids Surf. A Physicochem. Eng. Asp.* **2020**, *594*, 124653. [[CrossRef](#)]
35. Hussien, M.S.A.; Yahia, I.S. Hybrid multifunctional core/shell g-C₃N₄@TiO₂ heterojunction nano-catalytic for photodegradation of organic dye and pharmaceutical compounds. *Environ. Sci. Pollut. Res.* **2021**, *28*, 29665–29680. [[CrossRef](#)] [[PubMed](#)]
36. Deng, S.Z.; Yang, G.L.; Zhu, Y.H.; Li, F.W.; Zhang, X. WO₃ nanosheets/g-C₃N₄ nanosheets' nanocomposite as an effective photocatalyst for degradation of rhodamine B. *Appl. Phys. A Mater. Sci. Process.* **2019**, *125*, 1–11. [[CrossRef](#)]
37. Al-Ghamdi, A.A.; Khedr, M.H.; Ansari, M.S.; Hasan, P.M.Z.; Abdel-Wahab, M.S.; Farghali, A.A. RF sputtered CuO thin films: Structural, optical and photocatalytic behavior. *Phys. E Low-Dimens. Syst. Nanostructures* **2016**, *81*, 83–90. [[CrossRef](#)]
38. Zhao, C.; Ran, F.; Dai, L.; Li, C.; Zheng, C.; Si, C. Cellulose-assisted construction of high surface area Z-scheme C-doped g-C₃N₄/WO₃ for improved tetracycline degradation. *Carbohydr. Polym.* **2021**, *255*, 117343. [[CrossRef](#)]
39. Pan, T.; Chen, D.; Xu, W.; Fang, J.; Wu, S.; Liu, Z.; Wu, K.; Fang, Z. Anionic polyacrylamide-assisted construction of thin 2D-2D WO₃/g-C₃N₄ Step-scheme heterojunction for enhanced tetracycline degradation under visible light irradiation. *J. Hazard. Mater.* **2020**, *393*, 122366. [[CrossRef](#)]
40. Zhao, X.; Zhang, X.; Han, D.; Niu, L. Ag supported Z-scheme WO_{2.9}/g-C₃N₄ composite photocatalyst for photocatalytic degradation under visible light. *Appl. Surf. Sci.* **2020**, *501*, 144258. [[CrossRef](#)]
41. Yan, H.; Zhu, Z.Y.; Long, W.L. Single-source-precursor-assisted synthesis of porous WO₃/g-C₃N₄ with enhanced photocatalytic property. *Colloids Surf. A Physicochem. Eng. Asp.* **2019**, *582*, 123857. [[CrossRef](#)]
42. Yoon, M.Y.; Oh, S.; Hong, J.S.; Lee, R.; Boppella, S.H.K.; Mota, F.M.; Kim, S.O.; Kim, D.H. Synergistically enhanced photocatalytic activity of graphitic carbon nitride and WO₃ nanohybrids mediated by photo-Fenton reaction and H₂O₂. *Appl. Catal. B Environ.* **2017**, *206*, 263–270. [[CrossRef](#)]